

Surface-Template Assembly of Two-Dimensional Metal–Organic Coordination Networks

Sebastian Stepanow,[†] Nian Lin,^{*,†} Johannes V. Barth,^{*,§} and Klaus Kern^{†,‡}

Max-Planck-Institut für Festkörperforschung, Heisenbergstrasse 1, D-70569 Stuttgart, Germany, Institut de Physique des Nanostructures, Ecole Polytechnique Fédérale de Lausanne, CH-1015 Lausanne, Switzerland, and Advanced Materials and Process Engineering Laboratory, Departments of Chemistry and Physics & Astronomy, The University of British Columbia, Vancouver, British Columbia V6T 1Z4, Canada

Received: August 7, 2006; In Final Form: September 13, 2006

The self-assembly of iron-coordinated two-dimensional metal–organic networks on a Cu(100) surface has been investigated by scanning tunneling microscopy under ultra-high-vacuum conditions. We applied three rodlike polybenzene dicarboxylic acid molecules with different backbone lengths as organic linkers. The three linker molecules form topologically identical rectangular networks with Fe, all comprising iron pairs as the network nodes. Whereas the length of the linker molecules defines the dimension of the networks, the substrate also significantly influences the structural details, e.g., network orientation with respect to the substrate, geometric shape of the network cavities, Fe–carboxylate coordination configuration, and iron–iron distance.

Introduction

The deliberate fabrication of materials with designed structures is an appealing and challenging goal from both scientific and technological points of view. Particularly successful synthesis strategies are based on principles of supramolecular chemistry.^{1–7} In the so-called bottom-up approach, the materials are built up from periodic repeated structures in the nanometer range by selective and directional noncovalent bonds, such as hydrogen bonds or metal–ligand interactions between the subunits.^{1–7} Metal coordination interactions are stronger, more directional, and more selective than hydrogen bonds and represent one of the most versatile and widely employed means to direct the organization of molecular building blocks. In particular, coordination complexes are interesting not only for the structural aspects but also for their intriguing functional properties, which one may exploit in the fields of catalysis, magnetism, and optical applications.^{8–27} The promise of these construction strategies for creating functional materials has already been demonstrated for different applications, such as second harmonic generation,^{15,16} gas storage, including size-selective sorption and molecular recognition,^{17–20} and catalysis,^{21–24} as well as applications to magnetic materials.^{8,25–27}

The coordination interaction has also been employed to construct supramolecular architectures at surfaces, offering the possibility to design low-dimensional organic–inorganic hybrid materials.^{28–32} These systems contain distinctly arranged transition metal units and two-dimensional (2D) cavities. In contrast to traditional coordination chemistry in three-dimensional (3D) solution phase, 2D confinement at the surface leads to rather uncommon metal coordination. In addition, the molecules and metal centers prefer certain adsorption sites on a substrate, which effectively influences the structures formed on top. Therefore, the coordination assembly principles applied to 3D structures are often modified, and a detailed understanding of the substrate

effects is required in order to establish the design principles of the 2D coordination assembly.

Here we report on scanning tunneling microscopy (STM) investigations focusing on self-assembly of metal–organic coordination networks at a Cu(100) surface. Three rodlike, symmetric polybenzene dicarboxylic acids, 1,4-benzoic acid (terephthalic acid, TPA), 4,4'-biphenyldicarboxylic acid (BDA), and 4,1',4'',1''-terphenyl-1,4''-dicarboxylic acid (TDA), shown in Figure 1, are used in the present study. Because the three molecules possess the same functional endgroups, it is expected that 2D networks of an analogue structure should evolve if the substrate influences are neglected. We indeed have observed that all three linker molecules form reticular 2D open coordination networks of a rectangular topology. However, there are marked differences in the coordination configurations and network geometries. Based on the high-resolution STM data and structural modeling, we point out that these differences are induced by substrate template effects.

Experimental Section

The sample preparation and STM measurements were carried out in an ultra-high-vacuum (UHV) environment, providing well-defined conditions for the experiments. The UHV chamber is equipped with standard facilities for surface preparation. The Cu(100) surface was prepared by several cycles of sputtering with argon ions and subsequent annealing at 800 K. The STM images were acquired at room temperature in the constant current mode with bias voltages in the range from a few millivolts up to 1.5 V. The commercially available molecules TPA (Fluka Chemie AG, purity >99%) and BDA (Sigma-Aldrich, purity 97%) and the specially synthesized TDA molecule,³³ all in powder form, were deposited by organic molecular beam epitaxy from a Knudsen-cell-type evaporator. The molecules were sublimated at 440, 490, and 530 K for TPA, BDA, and TDA, respectively. Iron (MaTeck GmbH, purity >99.99%) was deposited using an electron-beam heating evaporator (Omicron EFM 3). The employed deposition rates were in the range of a few percent of a monolayer per minute for both molecules and iron.

* Corresponding author. Telephone: 0049-711-6891617. Fax: 0049-711-6891662. E-mail: n.lin@fkf.mpg.de.

[†] Max-Planck-Institut für Festkörperforschung.

[‡] Ecole Polytechnique Fédérale de Lausanne.

[§] The University of British Columbia.

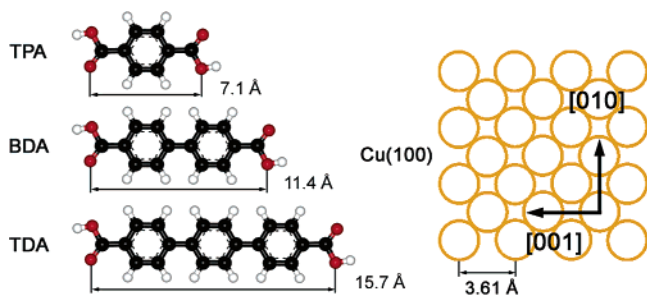


Figure 1. The three linker molecules. Distances between the two terminating carboxylic groups are given. The atomic structure of a Cu(100) surface is drawn on the same scale.

Upon adsorption on the substrate held at above or equal room temperature, all three molecules form densely packed and well-ordered molecular adlayers with fully deprotonated carboxylate moieties, as reported in our previous publications.^{34,35} In the remaining part of the paper, the abbreviations TPA, BDA, and TDA refer to the deprotonated species. The iron was deposited after the molecules' deposition in order to minimize Fe exchange with the copper surface. The substrate was held at temperatures in the range from 400 to 450 K during the iron deposition. The sample was then annealed at the same temperature for at least 5 min to facilitate the self-assembly process. In the case of BDA and TDA, a substrate temperature of 475 K was also used. Networks were observed after the Fe deposition and the annealing.³⁰ In general, we obtained better results for the network formation at higher annealing temperatures, i.e., an increasing domain size and a lower defect concentration. In particular, the evolution of well-ordered network domains of the long molecules BDA and TDA requires a higher preparation temperature compared to that of TPA. In addition, no dependence of the network topology on the metal–ligand concentration ratio was found for BDA and TDA, as it was observed for TPA (i.e., the mononuclear and row phases are encountered exclusively for the latter).³⁰

The molecular geometries of TPA, BDA, and TDA we used in structural modeling were calculated for isolated molecules in the PM3 approximation.^{36,37} In the models, we assume an unrelaxed molecular geometry. Recent DFT calculations show that the C–C bond relaxation of chemisorbed benzene on a Cu(100) surface results in a bond length increase of less than 2% and can be neglected for the rough determination of intermolecular distances.³⁸ Furthermore, we also neglect the local relaxation of the Cu substrate.

Results

(I) TPA Networks. TPA forms various types of binding motifs with Fe, depending on the Fe–TPA concentration ratios and subsequent annealing temperatures. A comprehensive description can be found in our previous paper.³⁰ For comparison, we focus here on the network structures containing Fe–Fe units. As depicted in Figure 2, the network nodes comprise Fe–Fe units that are surrounded by four carboxylate ligands. The TPA molecules align symmetrically with respect to the Fe–Fe units, i.e., two ligands at the bridging positions (normal to the Fe–Fe axis) and two at the axial positions (collinear with the Fe–Fe axis). The bridging ligands bind symmetrically to the two Fe atoms in a monodentate configuration, while the axial ligands form bidentate bonds to one Fe atom. Each iron atom is thus coordinated by four carboxylate oxygen atoms in a distorted square-planar geometry. The Fe–O distance is taken from the models and amounts to 2.0 ± 0.2 Å, which falls in

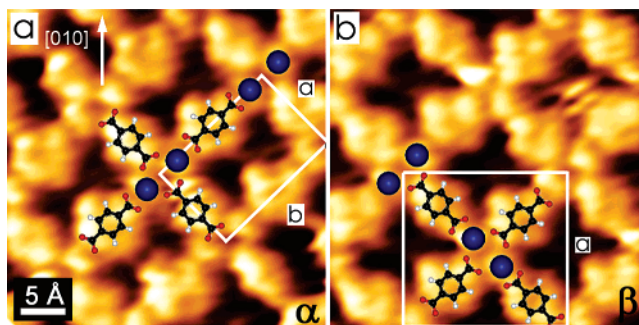


Figure 2. STM topographs of the Fe–TPA networks: (a) α -phase and (b) β -phase. Tentative models and the unit cells of the Fe–Fe arrays are superimposed on the STM topographs.

the range of the typical Fe–carboxylate coordination bond length.³⁹ The Fe–Fe axis is aligned along the $[0 -1 1]$ or $[0 1 1]$ substrate direction. The Fe–Fe spacing has been determined from the STM data as 4.7 ± 0.1 Å (the given error represents the standard deviation). The long axis of the TPA also follows the $[0 -1 1]$ or $[0 1 1]$ substrate direction. There are two types of structures that differ in the relative orientation of the adjacent Fe–Fe units. In the phase shown in Figure 2a, henceforth denoted as the α -phase, all Fe–Fe units have the same orientation. The Fe–Fe units form a rectangular lattice with a unit cell of $10.2 \text{ Å} \times 15.3 \text{ Å}$, which corresponds to $4a_0 \times 6a_0$ ($a_0 = 2.55$ Å being the nearest-neighbor atomic spacing of Cu(100)). The rectangular cavities expose an area of 25 Å^2 of the Cu substrate. In the second arrangement, represented in Figure 2b and denoted as the β -phase, the orientation of the Fe–Fe units alternate by a rotation of 90° with respect to the adjacent Fe–Fe unit. A square unit cell of the Fe–Fe centers with a size of $18.1 \text{ Å} \times 18.1 \text{ Å}$ ($5a_B \times 5a_B$, where $a_B = (2^{1/2})a_0 = 3.61$ Å is the Cu bulk cubic lattice constant) is formed, as drawn in Figure 2b. The cavities possess a square shape with an area of 35 Å^2 . In the α -phase, the linker molecules fall in two categories: the first type offers bridging ligands at both ends, and the second type offers axial ligands at both ends. In contrast, all the linker molecules in the β -phase are equivalent; i.e., each molecule offers a bridging ligand at one end and an axial ligand at the other end. The α - and β -phases are isomeric phases, coexisting on the surface in an equal ratio.

(II) BDA Networks. The BDA linkers form three distinct network phases with Fe, coexisting under the same conditions. Figure 3a shows an overview STM topograph, where the three phases are denoted as α , α' , and β , respectively, and the area at the upper-left corner (marked by an M) is a domain formed by the molecular BDA.³⁵ The α' - and β -phases can form extended domains, whereas the α -phase domains are much smaller and appear considerably less frequently; i.e., only very rarely does it consist of more than three rows.

All three phases have a rectangular topology, but the detailed structures differ in the orientation of adjacent Fe–Fe units, Fe–Fe spacing, and Fe–carboxylate coordination configuration. In the α -phase, depicted in the high-resolution STM image shown in Figure 3b, all Fe–Fe units align parallel, the same as the TPA α -phase. Note that the Fe–Fe axis follows the $[0 0 1]$ substrate direction, which is rotated by 45° with respect to the Fe–Fe units in the TPA phases. The molecular linkers are also rotated by 45° . The distance between two iron atoms amounts to 4.1 ± 0.3 Å, which is smaller than the Fe–Fe spacing in the Fe–TPA structures. The Fe coordination is remarkably different from what has been found in the Fe–TPA networks. First, the axial ligand molecules do not lie collinear with respect to the Fe–Fe axis; i.e., they are shifted (up or down, as shown in

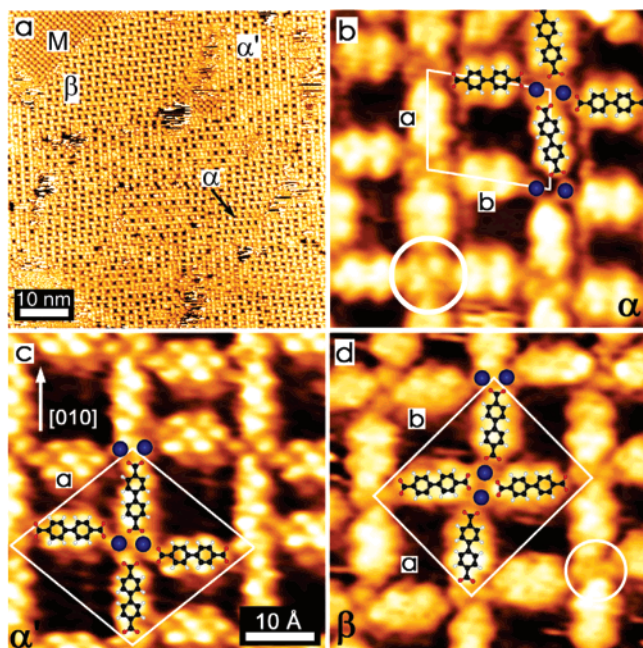


Figure 3. STM topographs of the Fe–BDA networks. (a) An overview showing the coexistence of the molecular phase (M) and the α -, α' -, and β -phases. (b–d) High-resolution data of α -, α' -, and β -phases. (All three images have the same scale.) The circles in (b) and (d) mark defect features.

Figure 3b) by ~ 1.8 Å. The shifting produces a staircase arrangement of the axial linker molecules, with a step of 3.6 Å (equal to the Cu bulk lattice constant a_B). Another new feature is that the long axis of the bridging linker molecules is tilted by about 10° with respect to the $[0\ 1\ 0]$ axis, so the bridging ligands do not point perpendicular to the center of the Fe–Fe units. As shown in Figure 3b, the upper apex of the molecule points to the left-side Fe and the lower apex to the right-side Fe of the Fe–Fe units. This arrangement indicates that the carboxylate groups cannot bridge the Fe–Fe units symmetrically, as illustrated by the superimposed model. The iron coordination will be discussed in detail below. The unit cell of the Fe–Fe array is a rhomboid, as drawn in Figure 3b, with $a = 14.4$ Å and $b = 18.4$ Å. The open cavities have a rhomboid shape with a size of 90 Å².

The α' -phase is depicted in Figure 3c. The Fe–Fe spacing amounts to 3.7 ± 0.1 Å, significantly smaller than the value in the α -phase. Similar to those in the α -phase, the axial ligands are not collinear to the Fe–Fe axis. However, in contrast to the staircase arrangement in the α -phase, the up- and down-shifting

of the axial ligands is opposite for adjacent nodes, resulting in the formation of consecutive wide and narrow rectangular cavities, 145 Å² and 55 Å² in size, respectively. In this particular STM image, the inner feature of the BDA molecule is resolved: The axial molecules show seven protrusions, in which the three central protrusions may be assigned as carbon–carbon single bonds and the two side protrusions at each side may be assigned to the aromatic carbon–carbon bonds. The bridging linker molecules have an asymmetric shape; i.e., at one side the protrusions are much dimmer. This could be an indication of a nonflat adsorption geometry. An influence of the scan direction can be excluded because the rotational domains show the same features. The bridging linker molecules are perpendicular to the Fe–Fe axis but shifted laterally, so the apexes do not point to the middle of the Fe–Fe units but rather close to one Fe in the Fe–Fe units. A detailed inspection reveals a correlation between the shifting of the bridging and the axial ligands: the bridging ligand is always shifted laterally toward the larger void (cf. Figure 3c). As drawn in Figure 3c, the α' -phase possesses a diamond-shaped Fe–Fe unit cell, with $a = b = 23.1$ Å.

The β -phase is shown in Figure 3d. Similar to the TPA β -phase, the Fe–Fe orientation alternates 90° in this phase. Each linker molecule offers a bridging ligand at one end and an axial ligand at the other end. The binding configuration of the Fe–Fe units is very close to that of the α -phase. The Fe–Fe distance is found to be 4.1 ± 0.3 Å, the same as that of the α -phase. The rectangular unit cell has dimensions of $a = 20.4$ Å and $b = 25.5$ Å. The area of the cavities is 90 Å².

(III) TDA Networks. Two TDA–Fe network structures coexist under identical experimental conditions. Similar to the previous two molecules, the adjacent Fe–Fe units either have the same orientation (α -phase) or alternate by a rotation of 90° (β -phase). Besides the 90° rotational domains, two types of α -phase exist, which have slightly different orientations with respect to the substrate, as shown in Figure 4a. These two phases enclose an angle of about $4.8^\circ \pm 0.3^\circ$, with the high-symmetry direction $[0\ 1\ 0]$ or $[0\ 0\ 1]$ as the bisecting line. The α -phase is encountered at least twice as frequently as the β -phase.

Structural details of the two TDA phases are shown in Figure 4b,c. The α -phase has a rhomboid-shaped Fe–Fe unit cell ($a = 18.8$ Å and $b = 23.7$ Å), with an open cavity exposing 260 ± 30 Å² of the Cu substrate. The binding configuration is similar to that of the Fe–BDA α -phase: the bridging linkers are tilted so that the bridging ligands do not point to the Fe–Fe units symmetrically; the axial ligands are displaced up or down off the Fe–Fe axis. The two slightly differently oriented α -phases

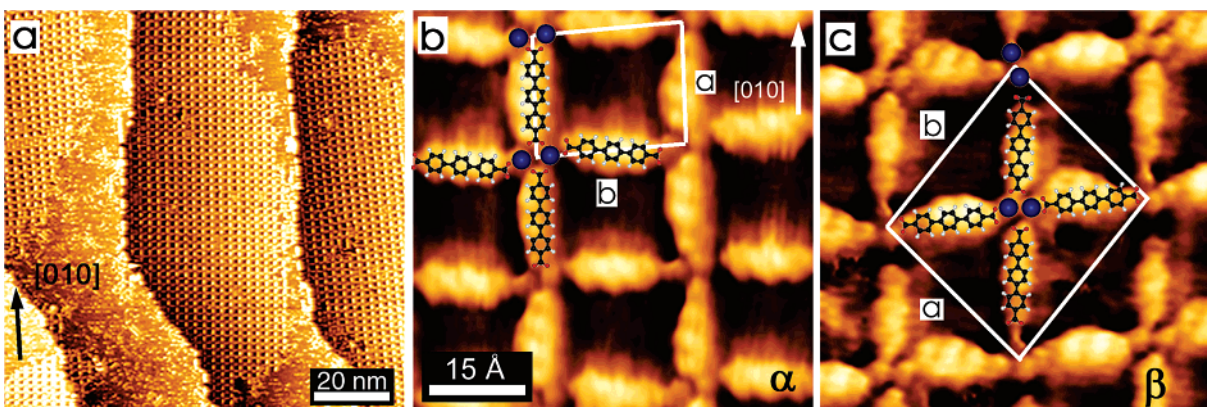


Figure 4. STM topographs of the Fe–TDA networks. (a) Large-scale image, showing two types of α -phase domains that orientate 2.4° with respect to the high-symmetry direction $[0\ 1\ 0]$. (b,c) High-resolution data of α - and β -phases (at the same scale).

TABLE 1. Summary of the Structural Parameters of the Observed Network Phases ($a_0 = 2.55 \text{ \AA}$)

structure	Fe-Fe unit cell			Fe-Fe		cavity	
	a (\AA)	b (\AA)	orientation	spacing (\AA)	orientation	exposed surface (\AA^2)	shape
TPA - α	10.2 ($4a_0$)	15.3 ($6a_0$)		4.7 ± 0.1	$[011]$ or $[0\bar{1}1]$	25	rectangle
TPA - β	18.1 ($5\sqrt{2} a_0$)	eq. to a		4.7 ± 0.1	$[011]$ and $[0\bar{1}1]$	35	square
BDA - α	14.4 ($4\sqrt{2} a_0$)	18.4 ($\sqrt{52} a_0$)		4.1 ± 0.3	$[010]$ or $[001]$	90	rhomboid
BDA - α'	23.1 ($\sqrt{82} a_0$)	eq. to a		3.7 ± 0.1	$[010]$ or $[001]$	145 & 55	rectangle
BDA - β	20.4 ($8 a_0$)	25.5 ($10 a_0$)		4.1 ± 0.3	$[010]$ and $[001]$	90	rhomboid
TDA - α	18.8	23.7		4.3 ± 0.2	$[010]$ or $[001]$	260 ± 30	rhomboid
TDA - β	27.5	31.1		4.3 ± 0.5	$[010]$ and $[001]$	220	rhomboid

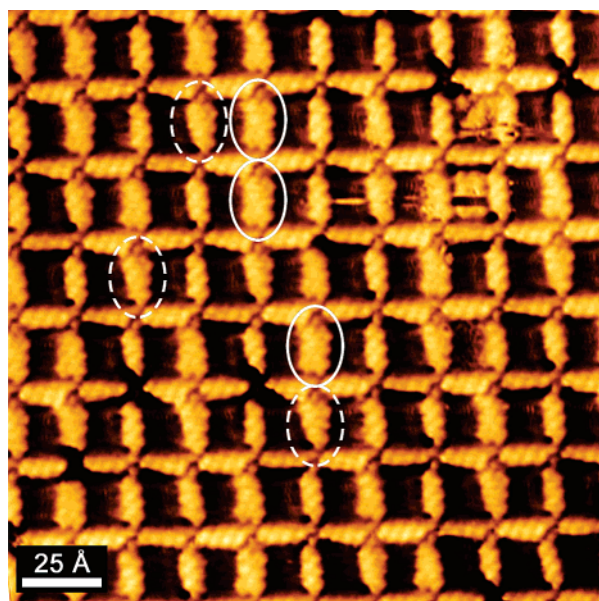


Figure 5. STM topograph of an Fe–TDA network domain showing the symmetrically (solid circles) and the asymmetrically (dashed circles) broadened molecules.

differ in their alignment of the axial ligands: in one phase, the left axial molecule is shifted downward and the right axial ligand is shifted upward at an Fe–Fe unit, as shown in Figure 4b; it is the opposite for the other phase. Thus, the two phases are mirror domains with respect to the $[0\ 1\ 0]$ or $[0\ 0\ 1]$ direction. In the β -phase, the Fe–Fe units form a large rhomboid unit cell ($a = 27.5 \text{ \AA}$ and $b = 31.1 \text{ \AA}$), as drawn in Figure 4c, where the area of the cavities is 220 \AA^2 . The iron–iron distance in both phases amounts to $4.3 \pm 0.5 \text{ \AA}$. The relatively large error

arises from a broad distribution of the Fe–Fe spacing. An analogy to the BDA α' -phase has not been observed.

The TDA α -phase exhibits an interesting feature: some of the linkers appear broadened (molecules marked by the solid circles in Figure 5) or asymmetric (i.e., one side is more broadened than the other side; molecules marked by the dashed circles in Figure 5). Because the width of the broadened features is too small for two parallel TDA molecules, we ascribe the broadening to molecular movement; i.e., these molecules are oscillating between two sites during the STM data acquisition. The frequency of the oscillation is higher than the STM scan speed, so the molecules appear as the smeared feature. Similar phenomena were reported previously in the literature.⁴⁰ If one end of a molecule is fixed while the other end is mobile, the molecule shows the asymmetric shape. The data also show that the oscillation always occurs at both axial positions of an Fe–Fe unit. This is corroborated by the fact that opposite axial ligands are always shifted in an anti-phase manner, indicating that the molecules presumably oscillate in opposite directions. The oscillations cause the large variation of the cavity size ($\Delta = 30 \text{ \AA}^2$).

Discussion

Table 1 summarizes the structural parameters of the observed networks. Evidently, the Fe–TPA networks strictly follow the substrate lattice. The Fe–BDA networks are commensurate with the substrate as well. In contrast, the unit cells of the Fe–TDA networks cannot be unambiguously correlated to the substrate lattice. In particular, the angle of about 2.4° between the TDA α -phase main axis and the $[0\ 0\ 1]$ direction impedes adjacent Fe–Fe units from residing on the same adsorption site. These data clearly indicate that the substrate plays a significant role in the coordination assembly processes, because otherwise the

three networks would be expected to have equivalent structures of different dimensions. We propose that the network structures are determined by the interplay of molecular adsorption energy (E_M), Fe adsorption energy (E_{Fe}), and Fe–carboxylate binding energy (E_B). E_M determines energetically favored molecular adsorption sites and molecular orientations. The most-favored adsorption site of benzene at Cu(100) is a hollow site, with a bonding of about 0.68 eV,³⁸ which may be used to estimate the adsorption site, orientation, and energy of the ligand molecules TPA, BDA, and TDA. E_{Fe} favors Fe atoms adsorbing at hollow sites. Typical bonding strength of metal adatoms to metal surfaces falls in the range of $\sim 2\text{--}3$ eV,⁴¹ but it is weakened when the atoms are incorporated in coordination complexes.⁴² E_B defines the specific coordination geometry between Fe and the surrounding oxygen, in particular an Fe–O distance of ~ 2.0 Å. A recent DFT calculation reported ~ 1.0 eV bonding strength of Fe–carboxylate coordination at a gold surface.⁴³ Because of the similar strengths of E_M , E_{Fe} , and E_B , a subtle balance of these three factors determines the overall network structures. For TPA, these terms are optimized in the observed structures; i.e., Fe atoms and benzene rings of TPA sit at or very close to hollow sites, and meanwhile an ideal Fe–carboxylate coordination is achieved. For polybenzene molecules BDA and TDA, E_M is becoming more significant. In particular, the molecules align along the [0 1 0] or [0 0 1] direction to fulfill a hollow-site adsorption of the two/three benzene rings; thus, the networks are largely guided by these two orientations, rotating $\sim 45^\circ$ with respect to the TPA networks. However, in such a configuration, Fe atoms cannot sit at hollow sites while maintaining an ideal Fe–carboxylate coordination. Thus, the networks undergo structural relaxation in order to lower the total energy, resulting in the observed multiple phases and incommensurate structures. Nevertheless, thorough theoretical investigations are required to unravel the contribution of each term and to predict structures.

A square-planar Fe coordination can be postulated for TPA networks. The Fe coordination of the two longer molecules, BDA and TDA, is more complicated and cannot be deduced unambiguously from STM data. The common motif, where the axial ligands always occupy non-collinear positions with respect to the Fe–Fe axis, suggests two possibilities. First, supposing that all carboxylate groups lie in the same plane, a planar trigonal coordination geometry would evolve. Such configuration is very rare in 3D compounds. However, the surface contribution must be taken into account here. In addition, the second oxygen atom of the axial linkers may potentially form a hydrogen bond to the nearby bridging ligand, which may additionally stabilize this arrangement. The second scenario is a distorted tetrahedral coordination if the carboxylate moieties of the axial ligands are tilted out of plane. An exact model for the 3D coordination environment cannot be deduced from the STM data. Further studies are required to gain full insight into the coordination configuration.

With regard to the growth conditions, the three molecules differ mainly in the annealing temperature. The main driving force in the network formation is the appropriate bonding of the carboxylate groups to the iron under the constraints of specific adsorption sites for the iron atoms, the carboxylate oxygen, and the aromatic rings, where the latter is expected to play a larger role. The higher annealing temperature for BDA and TDA compared to TPA is a result of the reduced mobility for these molecules. The higher mass and the increased translation and rotation barriers of the longer ligands are considered to contribute to this reduction. Another reason can be an increased barrier for the evolution of long-range ordered

network domains because of the formation of intermediate metastable complexes. Because the molecules form well-ordered domains before iron deposition, the energy required to dissolve the molecular phase must also be taken into account. Generally speaking, the preparation temperature needs to be sufficiently high to provide an adequate mobility of the molecules and iron atoms as well as to remove unwanted bonding, like hydrogen bonds, or to correct mis-engaged Fe–carboxylate bindings.

Conclusions

We have studied the self-assembly of two-dimensional open network structures formed by TPA, BDA, and TDA and co-deposited iron on Cu(100). The size of the cavities increases almost 1 order of magnitude from the shortest (TPA) to the longest (TDA) linker. The network structures are determined by the subtle interplay between the coordination interactions between metal centers and carboxylate groups and the interactions of the linker molecules and Fe atoms with the substrate. The latter significantly affects the structural details of the networks, e.g., orientation, geometry, and iron–iron spacing. In principle, one may exploit the substrate effects to steer the coordination assembly and, more importantly, tune the local metal coordination environment by selecting proper substrates and linker molecules. It is worth pointing out that the metal centers that are coordinated in these different environments may possess distinct electronic properties, which might result in novel magnetic or catalytic properties.^{44,45}

References and Notes

- (1) Lehn, J.-M. *Supramolecular Chemistry, Concepts and Perspectives*; VCH: Weinheim, 1995.
- (2) Atwood, J. L.; Davies, J. E. D.; MacNicol, D. D.; Vögtle, F., Eds. *Comprehensive Supramolecular Chemistry*; Pergamon: Oxford, 1996.
- (3) Whitesides, G. M.; Mathias, J. P.; Seto, C. T. *Science* **1991**, *254*, 1312.
- (4) Philp, D.; Stoddart, J. F. *Angew. Chem., Int. Ed. Engl.* **1996**, *35*, 1154.
- (5) Leininger, S.; Olenyuk, B.; Stang, P. J. *Chem. Rev.* **2000**, *100*, 853.
- (6) Holliday, B. J.; Mirkin, C. A. *Angew. Chem., Int. Ed.* **2001**, *40*, 2022.
- (7) Moulton, B.; Zaworotko, M. J. *Chem. Rev.* **2001**, *101*, 1629.
- (8) Ruben, M.; Rojo, J.; Romero-Salguero, F. J.; Uppadine, L. H.; Lehn, J.-M. *Angew. Chem., Int. Ed.* **2004**, *43*, 3644.
- (9) Seidel, S. R.; Stang, P. J. *Acc. Chem. Res.* **2002**, *25*, 972.
- (10) Rao, C. N. R.; Natarajan, S.; Vaidyanathan, R. *Angew. Chem., Int. Ed.* **2004**, *43*, 1466.
- (11) Cotton, F. A.; Lin, C.; Murillo, C. A. *Acc. Chem. Res.* **2001**, *34*, 759.
- (12) Eddaoudi, M.; Moler, D. B.; Li, H.; Chen, B.; Reineke, T. M.; O’Keeffe, M.; Yaghi, O. M. *Acc. Chem. Res.* **2001**, *34*, 319.
- (13) Cui, Y.; Evans, O. R.; Ngo, H. L.; White, P. S.; Lin, W. *Angew. Chem., Int. Ed.* **2002**, *41*, 1159.
- (14) Yaghi, O. M.; O’Keeffe, M.; Ockwig, N. W.; Chae, H. K.; Eddaoudi, M.; Kim, J. *Nature (London)* **2003**, *423*, 705.
- (15) Lin, W.; Lin, W.; Wong, G. K.; Marks, T. J. *J. Am. Chem. Soc.* **1996**, *118*, 8034.
- (16) Facchetti, A.; Annoni, E.; Beverina, L.; Morone, M.; Zhu, P.; Marks, T. J.; Pagani, G. A. *Nat. Mater.* **2004**, *3*, 910.
- (17) Kiang, Y.-H.; Gardner, G. B.; Lee, S.; Xu, Z.; Lobkovsky, E. B. *J. Am. Chem. Soc.* **1999**, *121*, 8204.
- (18) Fletcher, A. J.; Cussen, E. J.; Prior, T. J.; Rosseinsky, M. J.; Kepert, C. J.; Thomas, K. M. *J. Am. Chem. Soc.* **2001**, *123*, 10001.
- (19) Eddaoudi, M.; Kim, J.; Rosi, N.; Vodak, D.; Wachter, J.; O’Keeffe, M.; Yaghi, O. M. *Science* **2002**, *295*, 469.
- (20) Rosi, N. L.; Eckert, J.; Eddaoudi, M.; Vodak, D. T.; Kim, J.; O’Keeffe, M.; Yaghi, O. M. *Science* **2003**, *300*, 1127.
- (21) Fujita, M.; Kwon, Y. J.; Washizu, S.; Ogura, K. *J. Am. Chem. Soc.* **1994**, *116*, 1151.
- (22) Yaghi, O. M.; Li, G.; Li, H. *Nature (London)* **1995**, *378*, 703.
- (23) Pan, L.; Ching, N.; Huang, X.; Li, J. *Inorg. Chem.* **2000**, *39*, 5333.
- (24) Seo, J. S.; Whang, D.; Lee, H.; Jun, S. I.; Oh, J.; Jeon, Y. J.; Kim, K. *Nature (London)* **2000**, *404*, 982.
- (25) Kahn, O. *Acc. Chem. Res.* **2000**, *33*, 647.

- (26) Srikanth, H.; Hajndl, R.; Moulton, B.; Zaworotko, M. J. *J. Appl. Phys.* **2003**, *93*, 7089.
- (27) Maspoch, D.; Ruiz-Molina, D.; Wurst, K.; Domingo, N.; Cavallini, M.; Biscarini, F.; Tejada, J.; Rovira, C.; Veciana, J. *Nat. Mater.* **2003**, *2*, 190.
- (28) Dmitriev, A.; Spillmann, H.; Lin, N.; Barth, J. V.; Kern, K. *Angew. Chem., Int. Ed.* **2003**, *42*, 2670.
- (29) Spillmann, H.; Dmitriev, A.; Lin, N.; Messina, P.; Barth, J. V.; Kern, K. *J. Am. Chem. Soc.* **2003**, *125*, 10725.
- (30) Lingenfelder, M. A.; Spillmann, H.; Dmitriev, A.; Stepanow, S.; Lin, N.; Barth, J. V.; Kern, K. *Chem.—Eur. J.* **2004**, *10*, 1913.
- (31) Stepanow, S.; Lingenfelder, M.; Dmitriev, A.; Spillmann, H.; Delvigne, E.; Lin, N.; Deng, X.; Cai, C.; Barth, J. V.; Kern, K. *Nat. Mater.* **2004**, *3*, 229.
- (32) Lin, N.; Stepanow, S.; Vidal, F.; Barth, J. V.; Kern, K. *Chem. Commun.* **2005**, 1681.
- (33) Campbell, T. W. *J. Am. Chem. Soc.* **1960**, *82*, 3126.
- (34) Stepanow, S.; Strunskus, T.; Lingenfelder, M.; Dmitriev, A.; Spillmann, H.; Lin, N.; Barth, J. V.; Wöll, Ch.; Kern, K. *J. Phys. Chem. B* **2004**, *108*, 19392.
- (35) Stepanow, S.; Lin, N.; Vidal, F.; Landa, A.; Ruben, M.; Barth, J. V.; Kern, K. *Nano Lett.* **2005**, *6*, 901.
- (36) Dewar, M. J. S.; Thiel, W. *J. Am. Chem. Soc.* **1977**, *99*, 4899.
- (37) Stewart, J. P. *J. Comput. Chem.* **1989**, *10*, 221.
- (38) Lorente, N.; Hedouin, M. F. G.; Palmer, R. E.; Persson, M. *Phys. Rev. B* **2003**, *68*, 155401.
- (39) King, R. B., Ed. *Encyclopedia of Inorganic Chemistry*; Wiley: Chichester, 1994.
- (40) Gimzewski, J. K.; Joachim, C.; Schlittler, R. R.; Langlais, V.; Tang, H.; Johanssen, I. *Science* **1998**, *281*, 531.
- (41) King, D. A.; Woodruff, D. P., Eds. *The Chemical Physics of Solid Surfaces, Vol. 8, Growth and Properties of Ultrathin Epitaxial Layers*; Elsevier: Amsterdam, 1997.
- (42) Seitsonen, A. P.; Lingenfelder, M. A.; Spillmann, H.; Dmitriev, A.; Stepanow, S.; Lin, N.; Kern, K.; Barth, J. V. *J. Am. Chem. Soc.* **2006**, *128*, 5634.
- (43) Clair, S.; Pons, S.; Fabris, S.; Baroni, S.; Brune, H.; Kern, K.; Barth, J. V. *J. Phys. Chem. B* **2006**, *110*, 5627.
- (44) Lee, D.; Lippard, S. J. *Inorg. Chem.* **2002**, *41*, 2704.
- (45) Andres, H.; Bominaar, E. L.; Smith, J. M.; Eckert, N. A.; Holland, P. L.; Münck, E. *J. Am. Chem. Soc.* **2002**, *124*, 3012.